KIF18B is a cell type–specific regulator of spindle orientation in the epidermis

Rebecca S. Moreci and Terry Lechler*
Department of Dermatology and Department of Cell Biology, Duke University, Durham, NC 27710

ABSTRACT **Proper spindle orientation is required for asymmetric cell division and the establishment of complex tissue architecture. In the developing epidermis, spindle orientation requires a conserved cortical protein complex of LGN/NuMA/dynein-dynactin. However, how microtubule dynamics are regulated to interact with this machinery and properly position the mitotic spindle is not fully understood. Furthermore, our understanding of the processes that link spindle orientation during asymmetric cell division to cell fate specification in distinct tissue contexts remains incomplete. We report a role for the microtubule catastrophe factor KIF18B in regulating microtubule dynamics to promote spindle orientation in keratinocytes. During mitosis, KIF18B accumulates at the cell cortex, colocalizing with the conserved spindle orientation machinery. In vivo we find that KIF18B is required for oriented cell divisions within the hair placode, the first stage of hair follicle morphogenesis, but is not essential in the interfollicular epidermis. Disrupting spindle orientation in the placode, using mutations in either KIF18B or NuMA, results in aberrant cell fate marker expression of hair follicle progenitor cells. These data functionally link spindle orientation to cell fate decisions during hair follicle morphogenesis. Taken together, our data demonstrate a role for regulated microtubule dynamics in spindle orientation in epidermal cells. This work also highlights the importance of spindle orientation during asymmetric cell division to dictate cell fate specification.**

Monitoring Editor
Karen Oegema
University of California, San Diego

Received: Jun 4, 2021
Revised: Aug 16, 2021
Accepted: Aug 20, 2021

INTRODUCTION

Spindle orientation is a fundamental biological process that contributes to asymmetric cell divisions and the formation of complex tissue architecture. Robust regulation of this process is essential for both the development and homeostasis of many tissues (Poulson and Lechler, 2012; Kulukian and Fuchs, 2013; Lu and Johnston, 2013). However, the mechanisms that regulate this process and connect spindle orientation to cell fate decisions in distinct tissue contexts remain incomplete.

In many cell types, spindle orientation/positioning requires a conserved cortical protein complex containing LGN/NuMA/dynein-dynactin that interacts with astral microtubules to properly orient the mitotic spindle. Previous work highlighted the necessity of dynein-dependent pulling for spindle oscillations, placement, and orientation. While targeting dynein to the cell cortex is sufficient to produce spindle oscillations, targeting both NuMA and dynein/dynactin to the cell cortex is required to produce asymmetric pulling forces to shift the mitotic spindle (Kotak *et al.*, 2012; Okumura *et al.*, 2018). In addition, there is a growing appreciation that precise control of microtubule dynamics is required for proper spindle orientation. Recent work in human osteosarcoma U2OS cells has shown that inhibition of the EB1-dependent plus-tip microtubule tracking protein GTSE1 is required to promote astral microtubule destabilization. As GTSE is inhibited, microtubule dynamic instability increases and enables astral microtubules to properly interact with the cell cortex and reposition the mitotic spindle during prometaphase (Bendre *et al.*, 2016; Singh *et al.*, 2021). Furthermore, the kinesin Kip3p, which acts as a microtubule depolymerase, promotes microtubule disassembly at the bud tip in budding yeast. Upon loss of Kip3p, microtubule length increased, resulting in mispositioning of the spindle pole body (Gupta *et al.*, 2006). The mammalian homologue of Kip3p, KIF18B, has also been implicated in spindle positioning (McHugh *et al.*, 2018). However, its role in spindle orientation and asymmetric cell divisions in intact tissue has not been examined.

This article was published online ahead of print in MBoC in Press (http://www.molbiolcell.org/cgi/doi/10.1091/mbc.E21-06-0291) on August 25, 2021.

*Address correspondence to: Terry Lechler (terry.lechler@duke.edu).

Abbreviations used: CDK1, cyclin-dependent kinase 1; DMSO, dimethylsulfoxide; E, embryonic day; EB1, end-binding protein 1; GFP, green fluorescent protein; GTSE1, G2 and S-Phase Expressed 1; K14, keratin 14; KD, knockdown; KIF18B, kinesin family member 18B; KO, knockout mRNA, messenger RNA; MTBD, microtubule binding domain; Neo, neomycin; NuMA, nuclear mitotic apparatus; RNA-seq, RNA sequencing.

Like Kip3p, KIF18B promotes microtubule catastrophe. In cultured mammalian cells, KIF18B is enriched at the plus tips of astral microtubules during mitosis, the microtubules that interact with the spindle orientation machinery (Lee *et al.,* 2010; Stout *et al.,* 2011; Tanenbaum *et al.,* 2011; Walczak *et al.,* 2016; van Heesbeen *et al.,* 2017). Intriguingly, KIF18B loss displays minimal effects on mitotic progression, therefore making mutants particularly viable resources for studying the role of microtubule dynamics during spindle positioning. Live imaging of HeLa cells demonstrated that the loss of KIF18B results in increased spindle movements and displacement from the cell center during mitosis. Additionally, KIF18B knockout (KO) HeLa cells exhibited more spindle rotation in the *z*-plane (McHugh *et al.,* 2018). These data support the idea that KIF18B is required for spindle positioning during cell division and that changes in microtubule dynamics can translate to defects in spindle positioning. However, the functional consequence of altered spindle positioning in this instance remains unclear. These models focused on roles of KIF18B in cells that exhibit nonpolarized planar divisions; however, its role in regulating spindle orientation in polarized epithelia has yet to be examined.

The mammalian epidermis is an important model for studying the mechanism and function of spindle orientations in vivo. During development of the mammalian epidermis, oriented divisions of basal progenitors drive morphogenesis of the stratified epithelium, which is necessary for generating a barrier that shields against environmental insults, prevents water loss, and regulates ion exchange (Smart, 1970; Lechler and Fuchs, 2005; Poulson and Lechler, 2010, 2012). Defects in spindle orientation disrupt normal epidermal development and can lead to issues with barrier formation, differentiation defects, hair growth, and neonatal lethality, thus underscoring the importance of this process (Williams *et al.,* 2011; Niessen *et al.,* 2013; Seldin *et al.,* 2016). The connection between spindle orientation and eventual cell fate in the epidermis has been demonstrated by both lineage tracing and live imaging (Poulson and Lechler, 2012; Box *et al.,* 2019). Oriented divisions have also been observed in other cell types within the epidermis and its appendages, including placode cells during hair follicle morphogenesis and the transit amplifying cells of the hair matrix (Rompolas *et al.,* 2012; Niessen *et al.,* 2013; Byrd *et al.,* 2016; Ouspenskaia *et al.,* 2016; Seldin *et al.,* 2016; Morita *et al.,* 2021). The hair placode is the first stage of hair follicle morphogenesis. In the hair placode, basal cells exclusively exhibit asymmetric divisions perpendicular to the underlying basement membrane. This division orientation was proposed to be necessary for physically placing nascent suprabasal daughter cells away from dermal Wnt cues, enabling daughter cells to acquire a different fate (Ouspenskaia *et al.,* 2016). However, physiological roles of oriented divisions in placode architecture and cell fate acquisition have not yet been shown.

Here, we examine the roles of KIF18B in both cultured keratinocytes and the developing epidermis. KIF18B mutants show an increase in both astral microtubule length and number as well as changes in microtubule dynamics. Furthermore, KIF18B colocalizes with spindle orientation machinery at the cell cortex. Using novel conditional loss-of-function mice, we demonstrate that KIF18B is required for spindle orientation during asymmetric cell division in hair placode compartments, but not in the interfollicular epidermis. Misorientation of placode spindles caused defects in cell fate decisions within the developing hair follicle. We propose that KIF18B regulates microtubule dynamics, enabling the spindle orientation machinery to properly interact with astral microtubules and align the mitotic spindle to promote robust cell fate decisions.

RESULTS

KIF18B is required for spindle alignment in cultured keratinocytes

To understand whether KIF18B is required for spindle alignment in keratinocytes, we first established control (*Kif18b*$^{floxed/floxed}$) and KIF18B KO (KIF18BKO; *Keratin-14Cre;Kif18b*$^{floxed/floxed}$) cell lines from neonatal mouse back skin. KO was established by use of a tissue-specific Keratin 14-Cre (*K14-Cre*) line to induced recombination in the basal layer of the developing epidermis (Vasioukhin *et al.,* 1999). Recombination of the gene between the loxP sites removed a portion of the kinesin motor domain and induced a frameshift mutation (Supplemental Figure 1A). Western blotting demonstrated the loss of the KIF18B protein in KO cell lines (Figure 1, A and B). To determine whether KIF18B was required for spindle orientation, we examined spindle alignment in control and KIF18BKO cultured keratinocytes. When keratinocytes cultured on laminin enter mitosis, they recruit spindle orientation machinery, such as NuMA, to a polarized cortical crescent (Seldin *et al.,* 2013, 2016). We defined the spindle alignment angle in each cell as the angle between a line connecting the two spindle poles and one that bisects the NuMA crescent on the cell membrane (Figure 1C). In control keratinocytes, the majority of cells divided with mitotic spindle angles within 15 degrees of the cortical NuMA crescent (Figure 1, D and F). Loss of KIF18B resulted in an increased frequency of misaligned spindles in KIF18BKO cells compared with controls (Figure 1, E and G). While loss of KIF18B does not cause complete randomization of spindle orientation like mutations in the cortical crescent machinery LGN, dynactin, or NuMA$^{\Delta MTBD}$, our data are consistent with KIF18B promoting the fidelity of spindle alignment (Williams *et al.,* 2011; Seldin *et al.,* 2016). The spindle orientation defect was also present in a second, independently isolated, KIF18BKO cell line, confirming that the spindle orientation defect was not due to experimental technique (Supplemental Figure 1, B–G). Notably, when KIF18B protein expression was restored with a full-length KIF18B tagged with a C-terminal green fluorescent protein (GFP), spindle alignment was rescued (Supplemental Figure 1, B–G). The expression of the KIF18B-GFP cell line mimics that of endogenous KIF18B, with some cells exhibiting more promiscuous expression along the spindle microtubules due to overexpression. Previous work determined that KIF18B's regulation of astral microtubules was required for spindle centering and stabilization in planar cell divisions (McHugh *et al.,* 2018). Our data establish a new role for KIF18B in promoting robust spindle orientation to polarized intrinsic cues in keratinocytes.

KIF18B regulates microtubule length and number in keratinocytes

Despite the defects in spindle orientation found in KIF18BKO cells, the localization of the spindle orientation machinery components NuMA and dynein/dynactin (marked by p150^{glued}, a subunit of dynactin) was normal (Supplemental Figure 2, A–J). Compared to controls, KIF18BKO cells recruited NuMA and p150^{glued} at similar percentages and similar levels, as marked by cortical fluorescence intensity as well as similar lengths along the cell cortex (Supplemental Figure 2, C–J), indicating that KIF18B more likely affects spindle orientation through a mechanism downstream of the localization of conserved cortical protein complex.

KIF18B promotes microtubule catastrophes in vitro (McHugh *et al.,* 2018). Consistent with this, we found that loss of KIF18B produced a dramatic increase in both the length and number of astral microtubules compared with control mitotic spindles (Figure 2, A–B′; Supplemental Figure 2, K–M). Quantitation of microtubule fluorescence intensity demonstrated that astral microtubule number

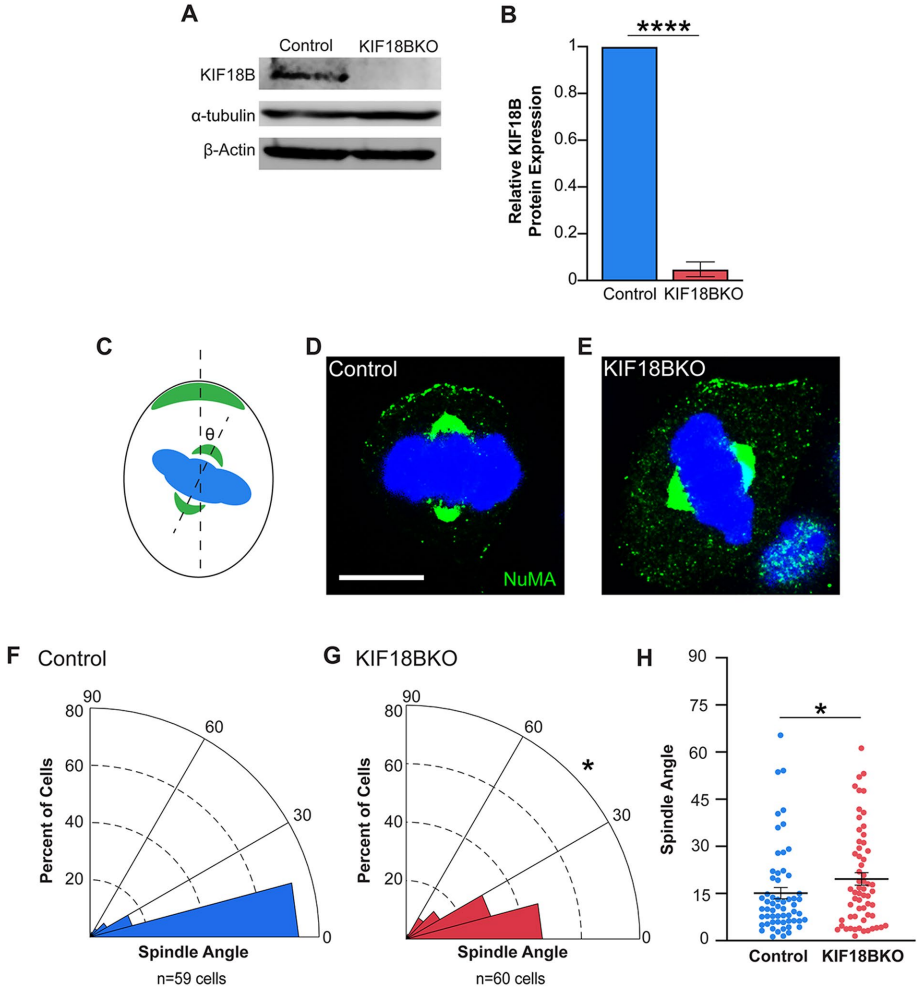

FIGURE 1: KIF18B is required for spindle orientation in cultured keratinocytes. (A) Western blot of proteins prepared from cell lysates for control and KIF18BKO keratinocyte cell lines. (B) Quantification of KIF18B protein levels in control and KIF18BKO ($n = 3$ individual experiments, $p < 0.0001$, Student's unpaired t test). (C) Diagram of spindle orientation measurement scheme with respect to cortical NuMA crescent (green). (D, E) Example images of spindle orientation with respect to NuMA (green) in control cells (aligned) and KIF18BKO cells (misaligned). (F, G) Radial histograms of spindle orientation in control (F) and KIF18BKO (G) cells (three individual experiments, 59 control cells and 60 KIF18BKO cells, $p = 0.0335$, Kolmogorov–Smirnov test). (H) Additional graphical representation of spindle alignment angles of control and KIF18B KO cells using a dot plot. Same data from F and G. Scale bars = 10 μm.

was greatly increased in the KO versus the control, whereas fluorescence intensity was unchanged in the spindle microtubules region, indicating that KIF18BKO predominantly affects astral microtubules (Figure 2B). The microtubule length in each astral region was increased between KO and control cells while the length of the spindle microtubule region was slightly shorter in KIF18BKO cells (Figure 2C; Supplemental Figure 2M). The total spindle length was increased overall due to the increase in astral microtubule length. Total spindle length was defined as the distance from the tip of each astral microtubule region to the tip of the opposite astral microtubule region. These data are in agreement with previous studies in other cell types (Stout *et al.*, 2011; Tanenbaum *et al.*, 2011; Walczak *et al.*, 2016; McHugh *et al.*, 2018). Both sides of the mitotic spindle were equally affected, as there was no difference in microtubule intensity or spindle length at either astral region with respect to the cortical NuMA crescent (Supplemental Figure 2, K–M) and KIF18B-GFP can partially rescue the spindle length (Supplemental Figure 2M).

KIF18B regulates microtubule dynamics during mitosis

To better characterize the effects that loss of KIF18B has on astral microtubule dynamics, we next turned to live imaging. We isolated primary mouse keratinocytes from both control and KIF18BKO neonatal mouse back skin. These mice also expressed an EB1-GFP transgene to visualize polymerizing microtubules (Muroyama *et al.*, 2016). KIF18BKO primary cells had more growing astral microtubules and longer astral microtubules compared with control cells. This became evident when examining the number of EB1 puncta in a single movie frame and standard deviation projections illustrating EB1 trajectories over time in KIF18BKO versus control cells (Supplemental Movies S1 and S2; Figure 3, A–C). Quantitation of the astral microtubules contacting the cell cortex revealed an almost 3× increase in the number of KIF18BKO cells (Figure 3C). We then tracked EB1-GFP comets to gain insight into microtubule dynamics. KIF18B loss resulted in astral microtubules with increased growth distance (total micrometers traveled), growth lifetime (seconds visible in movie), and growth speed (micrometers traveled/second) (Figure 3, D–F). These data are consistent with a decrease in microtubule catastrophes and demonstrate a requirement for KIF18B in regulating microtubule dynamics in keratinocytes.

KIF18B localizes to the cell cortex during mitosis in a NuMA-dependent manner

To better understand how KIF18B coordinates microtubule dynamics and spindle orientation, we turned to immunofluorescence staining. Immunolocalization of KIF18B in keratinocytes revealed a striking expression pattern; in addition to the astral microtubule tip localization that has been noted in other cell lines, we found that KIF18B localized to polarized crescents at the cell cortex during metaphase and notably colocalized with NuMA (Figure 4, A–C). Both the spindle pole and cortical localization were absent in KIF18BKO cells, demonstrating the specificity of the antibody. Previous studies have not reported this localization pattern, which may reflect that those studies used cell lines that do not undergo polarization and spindle orientation to internal cues.

Furthermore, KIF18B also colocalized with NuMA in anaphase. Previous work demonstrated that CDK1 phosphorylates NuMA during metaphase (Compton and Luo, 1995; Seldin *et al.*, 2013). At anaphase entry, as CDK1 is inactivated, NuMA becomes dephosphorylated, and localization expands along the cell cortex to become bipolar. The same localization pattern was observed for KIF18B (Figure 4, D–F).

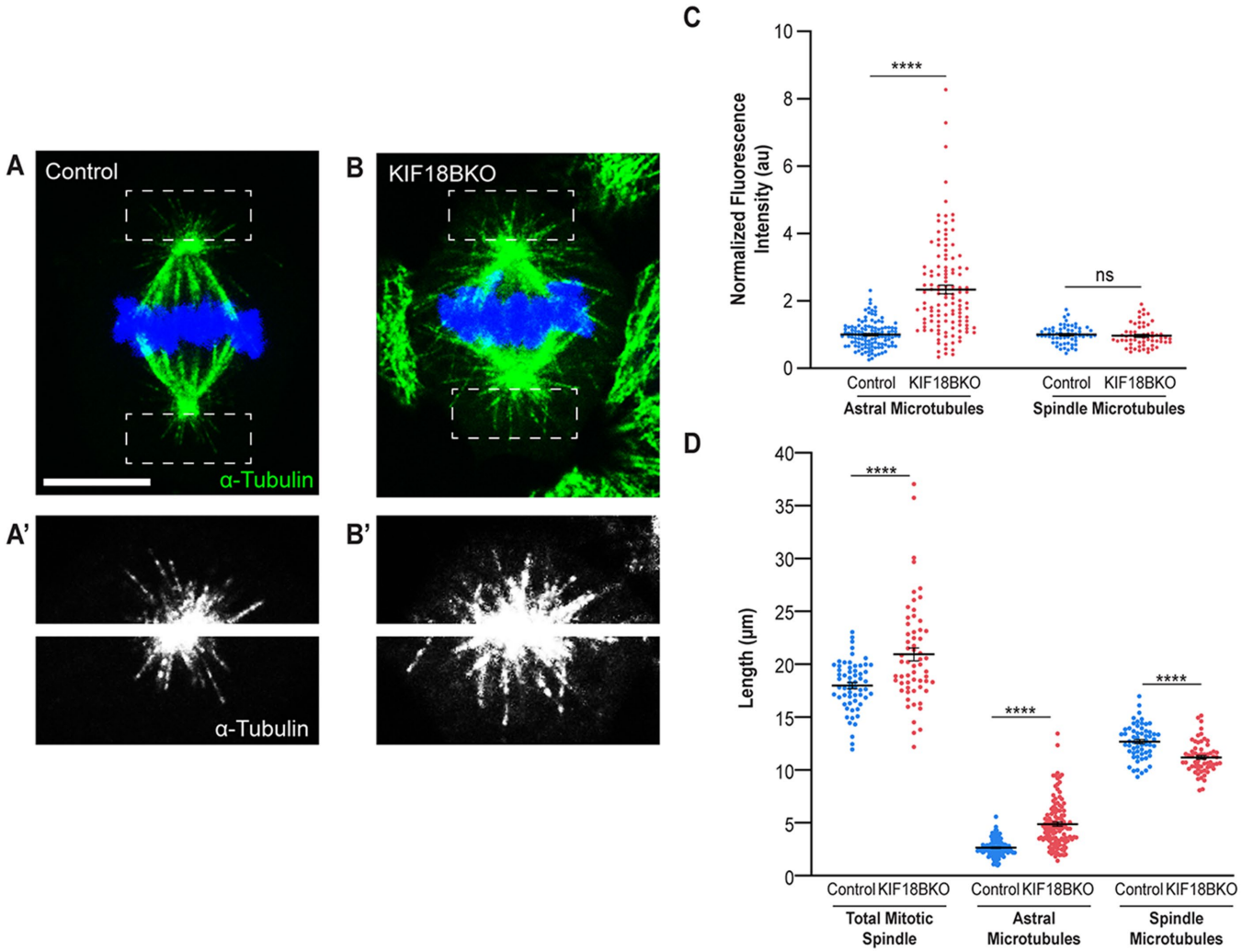

FIGURE 2: KIF18BKO alters spindle morphology in cultured keratinocytes. (A, B) Image of mitotic spindle during metaphase in KIF18BKO vs. control keratinocytes. α-Tubulin (green) labels microtubules. (A′, B′) Grayscale image of α-tubulin in control and KIF18BKO cells. Images are from dotted boxes of astral microtubule regions in A and B. (C) Quantification of microtubule fluorescence intensity at the indicated spindle location, normalized to control cell average (five individual experiments, $n = 60$ cells/condition, astral microtubules $p < 0.0001$, interpolar spindle $p = 0.5614$, Student's unpaired t test). (D) Quantification of spindle length at the indicated location (five individual experiments, $n = 60$ cells/condition, total mitotic spindle $p < 0.0001$, astral microtubules $p < 0.0001$, spindle microtubules $p < 0.0001$, Student's unpaired t test). Scale bar = 10 μm.

As this cortical localization pattern has not been previously observed, we wanted to further probe how KIF18B is recruited to the cell cortex. NuMA cortical localization during metaphase requires direct binding to LGN (Seldin *et al.*, 2013). We first utilized LGN knockdown (KD) (LGN KD) cells, which were previously created in the lab using validated short hairpin RNA (shRNA) constructs (Williams *et al.*, 2011; Seldin *et al.*, 2013). As expected, NuMA localization was absent at the cell cortex but was still present at the spindle poles during metaphase in LGN KD cells (Figure 5, A–C). KIF18B exhibited the same expression pattern; upon loss of LGN, KIF18B no longer localized to the cell cortex during metaphase, but it was still present at the spindle poles (Figure 5, A–C).

As previously stated, NuMA's localization is independent of LGN during anaphase, as CDK1 inactivation results in loss of NuMA phosphorylation, enabling it to bind directly to the cell membrane and accumulate in a bipolar manner along the cell (Compton and Luo, 1995; Seldin *et al.*, 2013). NuMA expression expanded along the cell cortex and was present at both cell poles in control and LGN KD cells (Figure 5, D–F). Again, KIF18B localization mimicked that of NuMA, as it was present at both cell poles and spindle poles in LGN KD cells (Figure 5, D–F). Consistent with the LGN-independent cortical localization of KIF18B and NuMA during anaphase, treatment of LGN KD cells with the CDK inhibitor purvalanol A mimicked anaphase onset and promoted cortical localization of both NuMA and KIF18B during metaphase (Supplemental Figure 3, A–C). These data suggest that like NuMA, KIF18B cortical localization is LGN dependent during metaphase but LGN independent during anaphase.

We next tested whether the cortical KIF18B localization during mitosis was dependent on NuMA by utilizing previously established shRNA NuMA KD (NuMA KD) cell lines (Williams *et al.*, 2011; Seldin *et al.*, 2013). In these cells, NuMA staining was greatly diminished (Figure 5, G–I). Further, KIF18B did not localize to either the cell cortex or the spindle poles, suggesting that KIF18B localization at both cell compartments is NuMA dependent. To test whether KIF18B cortical localization is dependent on microtubules, we

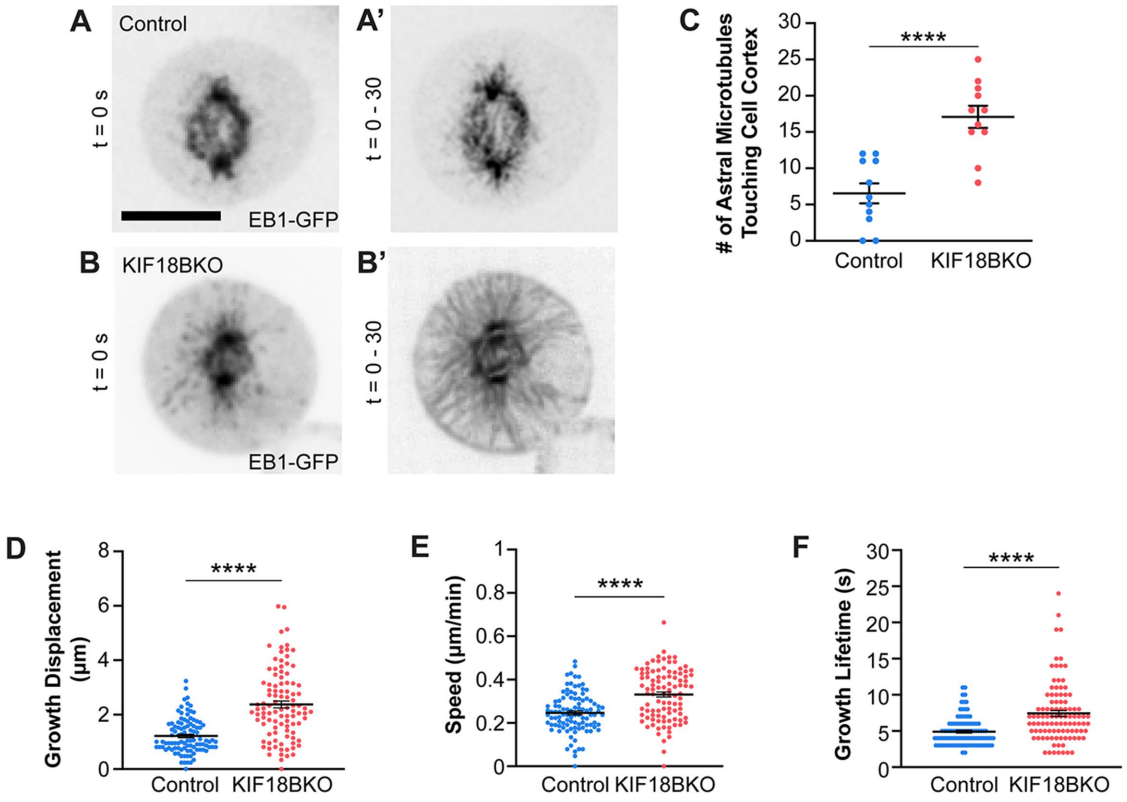

FIGURE 3: KIF18B regulates microtubule dynamics during mitosis. (A, B) Starting time point image ($t = 0$) for EB1-GFP puncta from spinning-disk movies in control and KIF18B KO cells. Movies are 30 s, 1 frame/second. (A′, B′) SD projections of 30 s movies. (C) Quantification of average number of astral microtubules touching the cell cortex in control and KIF18BKO cells (four individual experiments, $n = 11$ cells per condition, $p < 0.0001$, Student's unpaired t test). (D) Growth displacement of EB1-GFP comets over 30 s (four individual experiments, $n = 11$ cells per condition, $p < 0.0001$, Student's unpaired t test). (E) Speed of EB1-GFP comets over 30 s time period (four individual experiments, $n = 11$ cells per condition, $p < 0.0001$, Student's unpaired t test). (F) Growth lifetime of EB1-GFP comets in control and KIF18BKO cells (four individual experiments, $n = 11$ cells/condition, $p < 0.0001$, Student's unpaired t test). Scale bar = 10 µm.

treated cells with nocodazole to induce microtubule depolymerization. In dimethyl sulfoxide–treated cells, control keratinocytes maintained cortical localization of both NuMA and KIF18B (Supplemental Figure 3, D–F). In nocodazole-treated cells, spindle pole localization was disrupted, but cortical localization of both NuMA and KIF18B was preserved. Taken together, these data suggest that KIF18B localization at the cell cortex and spindle poles during mitosis requires NuMA. However, further investigation is needed to determine the function of cortical KIF18B and whether KIF18B binds directly to NuMA or forms a complex with additional proteins to promote its cortical localization.

Spindle orientation is required for hair follicle morphogenesis

The requirement of cortical spindle orientation machinery for asymmetric cell divisions during epidermal development is well documented (Williams *et al.*, 2011, 2014; Seldin *et al.*, 2016;). Loss of LGN, NuMA, or dynein/dynactin results in a range of phenotypes, from barrier defects to neonatal lethality. Our data demonstrate that KIF18B is required to properly regulate microtubule dynamics to control spindle alignment in cultured keratinocytes. These in vitro observations led us to investigate whether KIF18B also plays a role in regulating spindle orientation during epidermal development.

To understand the in vivo role of KIF18B in morphogenesis, we first examined KIF18B expression in the developing epidermis. During development, both the interfollicular epidermis and epidermal appendages, such as hair follicles, form in tandem (Figure 6A). Placodes are small epidermal thickenings that mark the first stage of hair follicle morphogenesis. Interestingly, KIF18B expression was enriched in hair placodes at embryonic day 16.5 (e16.5) during epidermal development (Figure 6, B and B′). Our KIF18B expression data are consistent with RNA-Seq data sets that also show placode enrichment compared with the interfollicular epidermis at the mRNA level (Sennett *et al.*, 2015; Rezza *et al.*, 2016). This is intriguing, as placode cells have been shown to exclusively divide asymmetrically, with the mitotic spindle perpendicular to the underlying basement membrane (Ouspenskaia *et al.*, 2016). These divisions were proposed to be functionally asymmetric, generating one slow-cycling basal cell and one suprabasal daughter cell marked by the transcription factor Sox9. Initial work proposed that Sox9^{positive} progenitors produce all lineages of the developing hair follicle, including the stem cell population within the bulge of the mature hair follicle (Nowak *et al.*, 2008; Ouspenskaia *et al.*, 2016). More-recent data suggest that the position of cells within the placode determines their cell fate and that Sox9^{positive} suprabasal placode cells do not directly produce stem cells of the mature hair follicle (Morita *et al.*, 2021). Nevertheless, the functional role and mechanistic control of

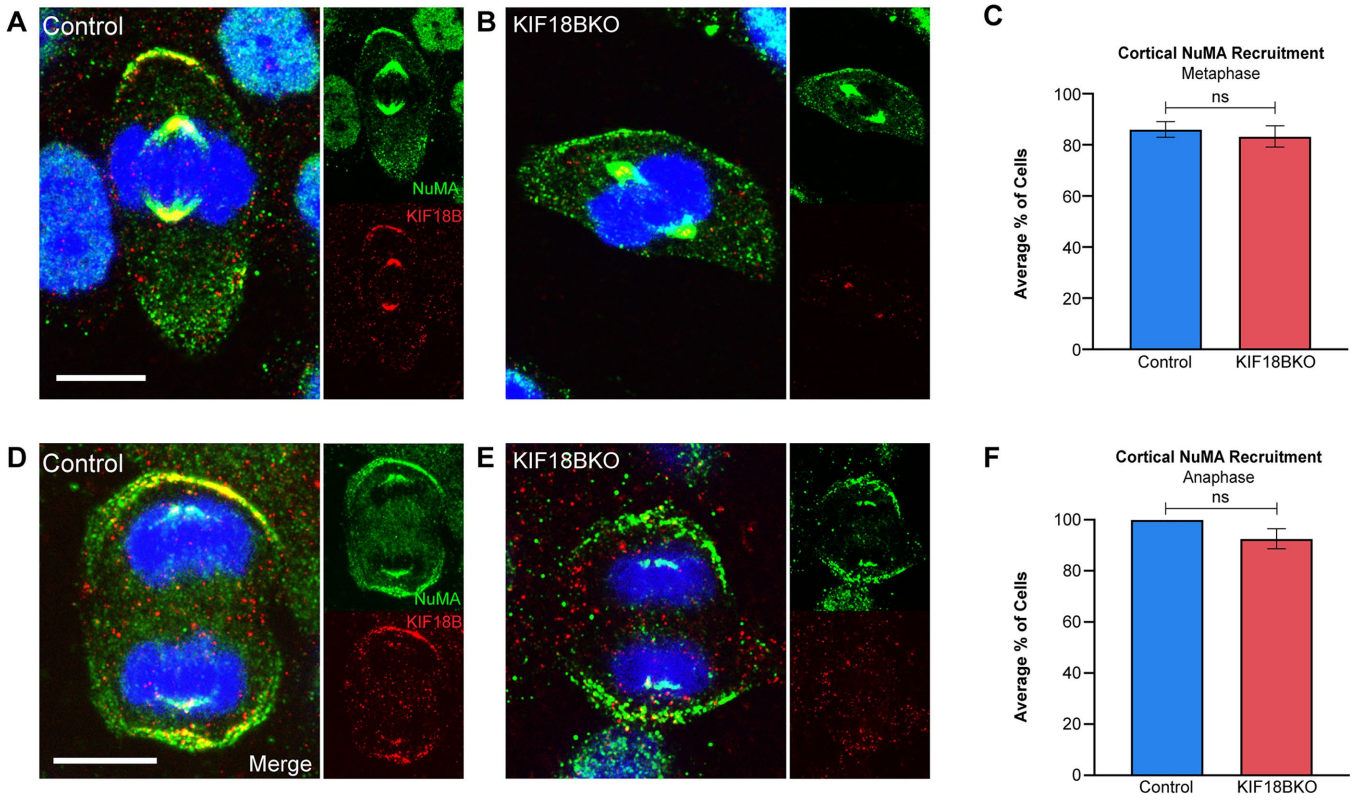

FIGURE 4: KIF18B accumulates at the cell cortex during mitosis. (A, B) Images of NuMA (green) and KIF18B (red) localization at the cell cortex in a crescent during metaphase. (C) Quantification of average percent of cortical protein recruitment in metaphase cells (three individual experiments, $n = 52$ cells/condition control cells, 48 KIF18BKO cells, $p = 0.6210$, Student's unpaired t test). (D, E) Images of NuMA (green) and KIF18B (red) localizing cortically at both poles of the cell during anaphase. (F) Quantification of average percent of cortical protein recruitment in anaphase cells (three individual experiments, $n = 39$ cells/condition, $p = 0.1301$, Student's unpaired t test). Scale bars = 10 μm.

these placode asymmetric cell divisions remain unclear. Notably, previous work demonstrated that LGN, which is essential for spindle orientation of interfollicular cells, was present in placode cells though not required for the orientation of hair follicle progenitors (Byrd *et al.*, 2016).

Next we assessed spindle orientation in both interfollicular and placode cells. We utilized the *K14-Cre;Kif18b*$^{fl/fl}$ and also the *K14-NuMA-GFP* transgenic line to mark spindle poles and facilitate quantitation of division angles. We examined spindle orientation at e17.5, a time point at which KIF18B is lost and at which the majority of spindles are perpendicular to the underlying basement membrane. In vivo, spindle orientation was measured by calculating the division angle of the two spindle poles (marked with NuMA-GFP) with respect to the basement membrane. Spindle orientation within the interfollicular epidermis was not statistically significantly different between KIF18B KO and control; the majority of divisions remained asymmetric with spindle angles between 60 and 90 degrees (Figure 6, E–G). This is consistent with the low levels of KIF18B expression in these cells. In contrast, when we examined spindle orientation in the hair placodes (using Sox2 labeling to identify these structures), we observed a clear role for KIF18B (Figure 6, C, D, and H–J). In control placodes, the majority of basal cells divided perpendicularly, as previously reported with division angles between 60 and 90 degrees (Figure 6, H and J) (Byrd *et al.*, 2016; Ouspenskaia *et al.*, 2016). Strikingly, KIF18BKO placodes contained basal cells dividing parallel to the basement membrane and across the spectrum of 0–90 degrees (Figure 6, I and J). Division angle did not correlate with position within the placode, as parallel-dividing cells were present both in the center and at the edges of placodes. This specific role for KIF18B in placode spindle orientation allows us to probe the functional role of these oriented divisions for the first time.

Previous studies proposed that division of Wnt^{high} basal cells away from the basement membrane is sufficient to drive changes in cell fate, establishing Sox9^{positive}/Wnt^{low} expression within suprabasal placode cells (Ouspenskaia *et al.*, 2016). This model assumed that cell fate specification is driven by external factors and that division into a Wnt^{low} environment instructs cell fate decisions. We tested this model using our conditional KO mouse. We first examined cell fate markers within control placodes. As expected, control placodes exhibited the stereotypical staining pattern, with Sox2 marking dermal condensates and the transcription factor Foxi3 marking basal placode cells. Sox9 nuclei were present within the suprabasal layer of the placode (Figure 6, K and L). Surprisingly, when we stained for these same markers in KIF18BKO mice, we observed Sox9 expression in the basal layer of the hair placode, an area from which it is normally absent (Figure 6M). To quantify this phenotype, we classified placodes as abnormal if they contained three or more Sox9^{positive} cells within the basal layer, as border placode cells display occasional Sox9 expression. In KIF18BKO mice 15–20% of placodes were mutant (Figure 6O). To understand whether this phenotype was specific to KIF18B mutants or a more general asymmetric cell division phenotype, we examined placodes in another asymmetric cell division mutant. We previously showed that a mutant of NuMA lacking its microtubule-binding domain (NuMA$^{\Delta MTBD}$) had defects in interfollicular spindle orientation (Seldin *et al.*, 2016). NuMA$^{\Delta MTBD}$ mutants demonstrated the same placode phenotype

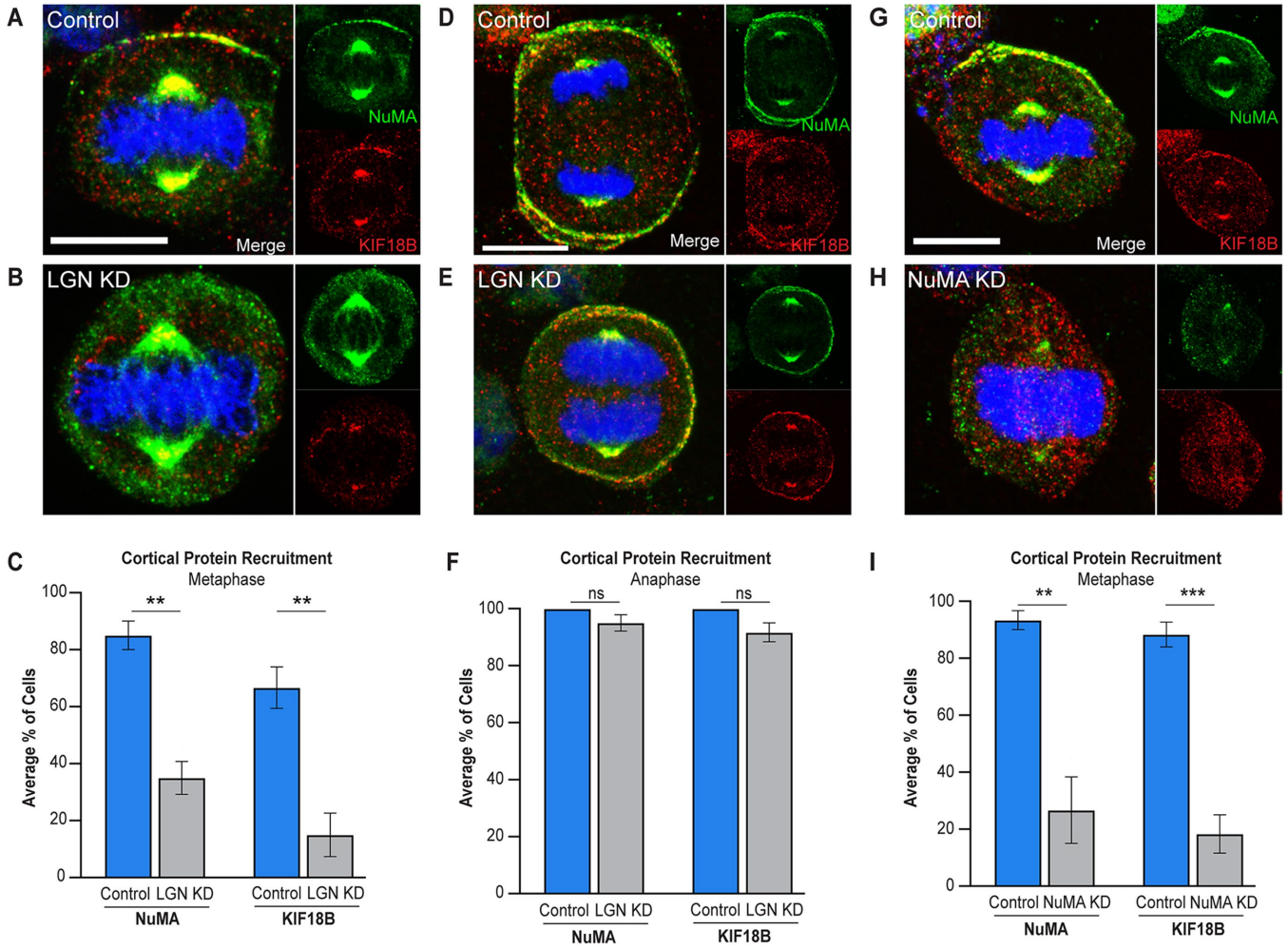

FIGURE 5: KIF18B localization requires spindle orientation machinery. (A, B) NuMA (green) and KIF18B (red) expression during metaphase in control and LGN KD cells. (C) Graph of the average percentage of metaphase cells with cortical NuMA and cortical KIF18B (three individual experiments, $n = 60$ cells/condition, NuMA $p = 0.0028$, KIF18B $p = 0.008$, Student's t test). (D, E) NuMA (green) and KIF18B (red) localization during anaphase in control and LGN KD cells. (F) Graph of the average percentage of anaphase cells with bipolar cortical NuMA and cortical KIF18B (three individual experiments, $n = 60$ cells/condition, NuMA $p = 0.1583$, KIF18B $p = 0.0668$, Student's t test). (G, H) NuMA (green) and KIF18B (red) localization during metaphase in NuMA KD vs. control cells. (I) Graph of the average percent of metaphase cells with cortical NuMA and cortical KIF18B (three individual experiments, $n = 60$ cells/condition, NuMA $p = 0.0053$, KIF18B $p = 0.0009$, Student's t test). Scale bars = 10 μm.

(40% of placodes abnormal, $n = 20$), with Sox9 expression expanding into the basal layer of the placode (Figure 6N). Taken together, these data suggest that disruption of spindle orientation and asymmetric cell division within hair placodes leads to changes in the architecture/organization of these structures, consistent with defects in asymmetric cell divisions and cell fate specification.

DISCUSSION

In this study, we characterized the role of the kinesin KIF18B in spindle orientation in keratinocytes and during skin and hair follicle morphogenesis. Loss of KIF18B increased astral microtubule length and number of astral microtubule cortical contacts and led to defects in spindle orientation in cultured keratinocytes. Intriguingly, KIF18B is specifically required for spindle orientation and cell fate specification in hair placodes but dispensable in the interfollicular epidermis, highlighting the requirement for distinct cortical machinery in different tissue contexts.

Our work demonstrates KIF18B's roles in controlling microtubule dynamics and spindle morphology in keratinocytes. Consistent with previous studies, disrupting KIF18B affected the morphology and dynamics of astral microtubules in epidermal keratinocytes (Lee *et al.*, 2010; Stout *et al.*, 2011; Tanenbaum *et al.*, 2011; Walczak *et al.*, 2016; McHugh *et al.*, 2018). KIF18BKO keratinocytes showed an increase in length and number of astral microtubules while EB1-GFP tracking revealed that astral microtubules contact the cell cortex more often in KIF18BKO cells than in control cells. EB1 puncta also exhibited larger growth displacements and growth lifetimes in KIF18BKO cells compared with controls. Taken together with the spindle orientation results, our data suggest that KIF18B promotes proper spindle orientation by modulating microtubule dynamics. Microtubule dynamics are also known to contribute to spindle positioning in other contexts, such as the one-cell stage of *Caenorhabditis elegans* development and budding yeast (Gupta *et al.*, 2006; Nguyen-Ngoc *et al.*, 2007).

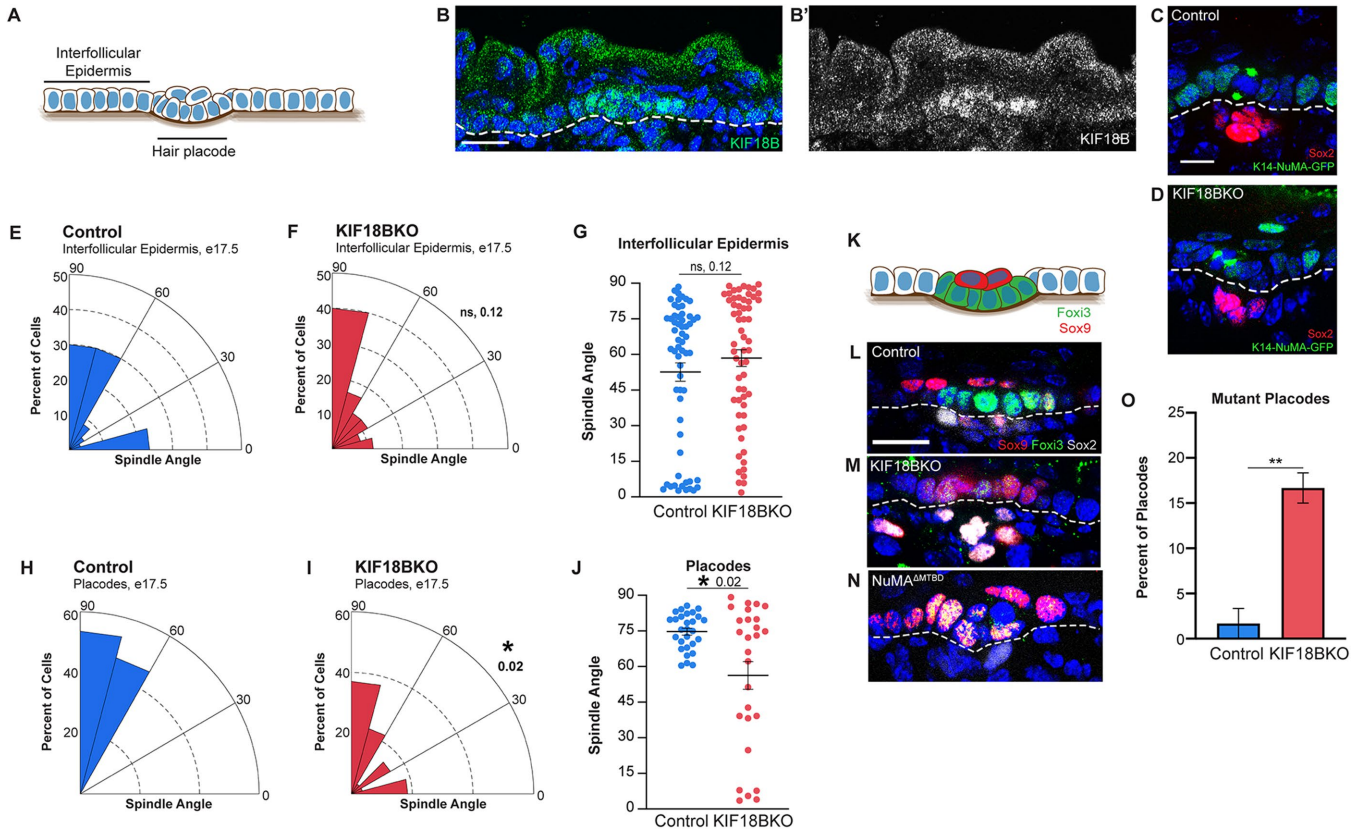

FIGURE 6: Spindle orientation is required for asymmetric cell division in hair placodes. (A) Diagram of interfollicular epidermis and hair follicle regions during early stages of hair follicle morphogenesis. The epidermis is depicted as a single layer for simplicity. (B) KIF18B (green) localization in hair placode at e16.5. Dotted line marks basement membrane. Scale bar is 20 μm. (C, D) Images of mitotic cells in control placode (C) and KIF18BKO placode (D). Sox2 (red) marks the dermal condensate while K14-NuMA-GFP (green) is used to measure spindle orientation with respect to basement membrane. Scale bar is 10 μm. (E, F) Radial histograms of spindle orientation in the back skin interfollicular epidermis of e17.5 mice (three separate pairs of mice from three litters, $n = 60$ control cells, 60 KIF18BKO cells, $p = 0.1196$, Kolmogorov–Smirnov test). (G) Additional graphical representation of spindle alignment angles of control and KIF18B KO cells using a dot plot. Same data from E and F. (H, I) Radial histograms of spindle orientation in placode cells of e17.5 epidermis (three separate pairs of mice from three litters, $n = 28$ control cells, 27 KIF18BKO cells, $p = 0.0209$, Kolmogorov–Smirnov test). (J) Additional graphical representation of spindle alignment angles of control and KIF18B KO cells using a dot plot. Same data from H and I. (K) Example diagram of cell fate markers in hair placode during development. Foxi3 (green) marks basal cells, and Sox9 (red) marks suprabasal cells. (L) Control placode showing marker localization for progenitor cells (Sox9, red), basal cells (Foxi3, green), and dermal condensate (Sox2, gray). Scale bar is 20 μm. (M, N) Abnormal placodes from KIF18KO (M) and NuMA$^{\Delta MTBD}$ (N). (O) Quantification of percent of mutant placodes in KIF18BKO compared with control (three separate pairs of mice from 3 litters, $n = 60$ placodes total per condition, $p = 0.0031$, *t* test).

In metazoans, the conserved cortical spindle orientation machinery generates pulling forces on astral microtubules to properly rotate the spindle into place (Lu and Johnston, 2013; Okumura *et al.*, 2018). Our data demonstrated that KIF18B colocalizes with the cortical spindle orientation machinery in keratinocytes. KIF18B localization mimics that of NuMA, requiring LGN for cortical localization during metaphase but not anaphase. KIF18B required NuMA to localize at both the spindle poles and the cell cortex during metaphase and anaphase. Whether KIF18B and NuMA bind directly to one another or form a complex with other proteins requires further investigation. However, this raises questions about whether coordination of microtubule dynamics locally at the cell cortex, globally throughout the cell, or both are required for proper spindle orientation. Future experiments aimed at specifically disrupting KIF18B's cortical localization should address this. Given that NuMA's microtubule-binding domain and interactions with astral microtubules are required for robust spindle orientation, it is intriguing to speculate that KIF18B's depolymerizing activity at the plus ends of astral microtubules can be co-opted by cortical machinery to guide spindle orientation and movement (Seldin *et al.*, 2016).

Previous work identified KIF18B as a regulator of spindle positioning and centering in HeLa cells (McHugh *et al.*, 2018). That work suggested that KIF18B is necessary for the planar alignment of the mitotic spindle with the underlying substrate. However, until now, KIF18B's role in regulating spindle orientation in cells that undergo polarized, asymmetric cell divisions had not been tested. We demonstrated that KIF18B is required for spindle orientation in cultured keratinocytes. However, we found no role for KIF18B in the planar or perpendicular divisions within the interfollicular epidermis. This is surprising for two reasons. First, the work in HeLa cells predicted that KIF18B would be required for planar spindle orientation of epithelial cells. Second, to our knowledge, KIF18B is the first example

of a protein that is required for spindle orientation in cultured keratinocytes but not in interfollicular epidermal cells in vivo.

In contrast, KIF18B has a clear role in spindle orientation in hair placodes during hair follicle morphogenesis. Previous research had observed oriented divisions in the placode, but the function and regulation of these divisions were not directly tested (Williams *et al.*, 2011; Ouspenskaia *et al.*, 2016). Interestingly, LGN is required for perpendicular spindles in the interfollicular epidermis but dispensable in hair placodes, while NuMA is required for both (Byrd *et al.*, 2016). These data emphasize the unique requirements for spindle orientation machinery among different subcompartments of the epidermis. Whether these distinctions reflect fundamental differences in microtubule dynamics or distinct regulators of microtubule dynamics between different pools of epidermal stem cells is a fascinating question that requires further attention.

The long-term effects of this mutant placode phenotype remain unclear and require further investigation. Hair follicle morphogenesis occurs in waves, with the first wave beginning around e12 or e13 (Saxena *et al.*, 2019). The K14-Cre promoter used here begins to turn on around e14.5, and proteins are lost by e15.5–16.5. Therefore, many hair placodes form before recombination, preventing us from exploring how KIF18B loss, and particularly disruptions in placode spindle orientation, impacts overall hair follicle morphogenesis. While we were generating the KIF18B floxed mouse line (*Kifb18*$^{fl/fl}$), we noted that KIF18B mice containing the Neo cassette acted as hypomorphs and displayed the same hair placode phenotype (KIF18B^{Neo}), even at earlier developmental time points (Supplemental Figure 4, A–C). Scenarios in which intact Neo cassettes disrupt regular gene expression have been well documented (Meier *et al.*, 2010; West *et al.*, 2016; Clark *et al.*, 2020). We were able to collect only a small number of these samples due to midembryonic lethality. However, these hypomorphs exhibited a decrease in the number of hair follicles at e18.5 (Supplemental Figure 4, D–F). This line does not allow us to determine whether this effect is cell autonomous, however, and future work is needed to determine the fates of placodes with disrupted patterning.

A current model suggests that oriented divisions out of a Wnt^{high} basal signaling hub are sufficient to drive cell fate changes in the placode (Ouspenskaia *et al.*, 2016). In support of this, recent work identified asymmetric secretion of both Wnt repressors and activators within the placode (Matos *et al.*, 2020). However, analysis of KIF18BKO placodes suggests novel modes of intrinsic control of cell fate in addition to extrinsic cues. In the mutant, Sox9 progenitor cells were present within the basal placode layer, adjacent to dermal Wnt signals. If cell fate control were under extrinsic control alone, these cells should have the correct fate. Furthermore, we were able to recapitulate expansion of Sox9 expression into the basal layer when treating mice with Porcupine inhibitor LGK974 (Supplemental Figure 4, G and H). Together, these data are consistent with a model in which Wnt regulators, whether repressors or activators, are asymmetrically inherited during oriented cell divisions to dictate cell fate specification. An alternative explanation is that KIF18B directly affects Wnt signaling. While we cannot rule this out, the fact that both NuMA and KIF18B mutants disrupt spindle orientation and cell fate acquisition suggests a more direct role for asymmetric cell divisions. This also highlights the importance of identifying asymmetrically inherited factors that influence these fate decisions. Collectively, our work demonstrates a functional role for regulated microtubule dynamics during asymmetric cell division and the importance of oriented divisions during epidermal development.

MATERIALS AND METHODS

Request a protocol through *Bio-protocol*.

Mice

All animal work was approved by Duke University's Institutional Animal Care and Use Committee. Mice were maintained in a clean, barrier facility with 12 h light/dark cycles. Both male and female mice were used in this study. Mice were genotyped by PCR to confirm strain before analysis. Mouse strains used in this study were Kif18b$^{fl/fl}$ (generated by Duke Transgenic and Knockout Mouse Shared Resource); Keratin 14-Cre (Vasioukhin *et al.*, 1999); K14-EB1-GFP (Muroyama *et al.*, 2016); Keratin 14-NuMA-GFP (Poulson and Lechler, 2010); and NuMA1-ΔMTBD (Silk *et al.*, 2009).

Cell culture

Keratinocytes were maintained at 37°C, 7.5% CO_2 and grown in E low-calcium medium. Cells were incubated with an additional 0.5 mM calcium for 4 h before experimental analysis. To produce primary keratinocytes, back skin was removed from mice at passage 0 to passage 3 (p0–p3) and placed in a 1:1 dispase II (Hoffmann-La Roche, Basel, Switzerland):1× phosphate-buffered saline (PBS) solution at 4°C overnight (O/N). Epidermis was then separated from the dermis and placed in a 1:1 mixture of versene/trypsin-EDTA (0.25%) for 12 min. Following incubation, cells were resuspended in medium, filtered (70 µm cell strainer), pelleted, and resuspended in medium before plating. For immediate experimental use, cells were plated on 3.5 mm glass-bottomed TC plates coated with laminin. Medium for primary cultures was supplemented with 0.5 mM calcium and dual SMAD inhibitors (Mou *et al.*, 2016). To create stable lines, cells were initially plated with 0.5 mM calcium onto fibroblast feeders. With each passage, calcium content was decreased by 0.1 mM until cells were able to be weaned off calcium and feeders. KIF18B control and KO cell lines were additionally grown with dual SMAD inhibitors.

LGN KD and NuMA KD cells were previously made in the lab using small interfering RNA constructs (Seldin *et al.*, 2013). Early passages (p0–p3) of both stable lines were used. Culture was supplemented with puromycin to maintain KD.

Phoenix cells were passaged at 37°C, 7.5% CO_2, grown in DMEM/10% fetal bovine serum (FBS) but switched to 32°C to produce retrovirus.

See Table 1 for detailed information on the chemicals and drugs used in this study.

Production of KIF18B-GFP construct and cell line

All PCR for cloning purposes was performed using Verifire DNA Polymerase. GFP was amplified from the pEGFP-C1 vector using forward primer 5′-TCGATGAATTCggtggcggtggctcgggcggaggtgggtcgATGGTGAGCAAGGGC-3′ and reverse primer 5′-TCGATGTCGACTTACTTGTACAGCTCGTC-3′ and then ligated into pBabe-puro vector (Addgene #1764) between the *Eco*RI and SalI sites. After the *Eco*RI site, the forward primer contained nucleotides encoding a 10-amino-acid flexible linker sequence (GGGGSGGGGS) between the KIF18B and GFP sequences. KIF18B was amplified from pEGFP-KIF18B (gift from Claire Walczak) using forward primer 5′-TCGATGGATCCGCCACCATGGCAGTGGAGGACAGC-3′ and reverse primer 5′-TCAGTGAATTCGTGCCAGTCACCTGG-3′ and inserted between the *Bam*HI and *Eco*RI sites. The stop codon was removed from the KIF18B C-terminal end. The primers were designed against *Homo sapiens* kinesin family member 18B (KIF18B), transcript variant 2, mRNA (NM_001264573.2) to produce the insert. Successful cloning was confirmed by DNA sequencing via Eton Biosciences (Research Triangle Park, NC).

Drug	Supplier	Catalog #	Use	Working concentration	Treatment time
A 83-01	Sigma-Aldrich	SML0788	Dual SMAD inhibitor cocktail	1 μM	Continuous
CHIR99021	Sigma-Aldrich	SML1046	Dual SMAD inhibitor cocktail	1 μM	Continuous
DMH-1	Sigma-Aldrich	D8946	Dual SMAD inhibitor cocktail	1 μM	Continuous
LGK974	Caymen Chemical	14072	Wnt inhibitor, IP injections	3 mg/kg	e15.75, e16.25
Nocodazole	Sigma-Aldrich	M1404	Depolymerize microtubules	10 μM	10 min
Puromycin	Amresco	J593-25MG	Selection for cell lines	2 μg/ml	Continuous
Purvalanol A	Tocris	1580	CDK inhibitor, Cell culture	100 μM	3 min
Y-27632	Selleck Chemicals	S1049	Dual SMAD I inhibitor cocktail	5 μM	Continuous

TABLE 1: Drug and chemical information.

Retrovirus was created using Phoenix cells, Mirus TransIT-LT1 reagent, and the provided protocol (Mirus Bio; MIR 2300). Virus was filtered with a 0.45-μm filter before use. To establish a stably expressing cell line, KIF18BKO cells (1 × 3.5 cm plate) were incubated with 2 ml of KIF18B-GFP retrovirus, polybrene (6 μg/ml), and FBS (9%*)* for 15 min at room temperature (RT). The plate was spun at 32°C in a benchtop centrifuge for 30 min at 1100 × *g*, rinsed 3 × 1× PBS, and then incubated with E low-calcium medium + dual SMAD inhibitors. Cells were passaged, expanded, and then selected using puromycin. After selection, cells were sorted for GFP+ expressors.

Immunoblots

Cells were lysed and collected on ice in RIPA buffer (50 mM Tris, pH 7.9, 150 mM NaCl, 0.5 mM EDTA, pH 8.0, 1% NP-40, 0.1% SDS, 0.5% sodium deoxycholate) with Protease Inhibitor Cocktail (Roche; 11697498001) and phenylmethylsulfonyl fluoride (1 mM; PanReacAppliChem; A0999). Samples were then rotated at 4°C for 30 min, sonicated for 3 × 10 s, and placed on ice in between rotations. Protein was separated from cellular debris via centrifugation (10 min, 15,000 × *g* at 4°C) and stored at –80°C.

Lysates were mixed 1:1 with loading buffer (15% β-mercaptoethanol, 10% SDS, 40% glycerol, and 3% bromophenyl blue) for protein gel analysis. Protein samples were then denatured by boiling for 5 min at 100°C and subsequently run on 7.5% polyacrylamide gels at 100 V for approximately 120 min. Proteins were then transferred from the gel onto nitrocellulose membranes at 100 V for 80 min. Following transfer, membranes were blocked with 5% bovine serum albumin (BSA) in PBS-T (2% Tween-20 in PBS) for 1 h. Membranes were then incubated O/N in primary antibodies, rocking at 4°C. Membranes were then washed 3 × 5 min in 1× PBS-T, incubated in secondary antibodies at room RT, rocking, for 1 h, and then washed 3 × 5 min in 1× PBS-T and visualized using a LI-COR Odyssey FC System. Primary antibodies (diluted in 5% BSA in 1× PBS-T) were as follows: mouse anti–β-actin (1:10,000; Sigma-Aldrich; A5441), rat anti–α-tubulin (1:2000; Santa Cruz; sc-53029), rabbit anti-KIF18B (1:500; Sigma-Aldrich; HPA024205), and chicken anti-GFP (1:5000; Abcam; ab13970). Secondary antibodies were Licor, IRDye 680RD Series or CW800 Series diluted 1:5000 in 5% BSA/1× PBS-T. For GFP antibody visualization, membrane was incubated with secondary goat anti-chicken horseradish peroxidase (1:5000 in 5% BSA/1× PBS-T; Jackson ImmunoResearch; 103-035-155) and then incubated for 2 min in the dark with ECL Western Blotting Substrate (ThermoFisher; PI-32106) before using the LI-COR system. The LI-COR system was used for quantifications. β-Actin was used as a loading control and compared with KIF18B for protein fold quantification.

Immunofluorescence

Tissue culture; sample collection through primary antibody. Cells were cultured on glass coverslips. For assays using spindle orientation machinery, cells were plated on laminin-coated coverslips (100 μM; Invitrogen; 23017015). Coverslips were quickly rinsed in warm 1× PBS and then fixed in ice-cold methanol (MeOH) for 3 min. MeOH-fixed coverslips were then rinsed with 1× PBS-T (0.2% Triton-X) for 5 min. For fixation of microtubules, coverslips were fixed in 37°C glutaraldehyde fixative (80 mM PIPES, pH 6.9, 50 mM NaCl, 2 mM $MgCl_2$, 0.2% Triton-X, 1% glutaraldehyde) for 10 min followed by rinsing with 1× PBS-T 3 × 5 min. Glutaraldehyde was then quenched with a small amount of sodium borohydride in PBS for 7 min followed by 3 × 5 min rinse in 1× PBS-T.

After rinses, cells were blocked with "Block" (3% BSA/5% normal donkey serum [NDS]/5% normal goat serum in PBS-T) or "NDS Block" (3% BSA/5% NDS in PBS-T) for 15 min. All antibodies were diluted in blocking solution and incubated at conditions indicated in Table 2. Following primary incubation, the coverslips were rinsed 3 × 5 min in PBS-T.

Mouse tissue; tissue collection through primary antibody incubation. Tissue was embedded in OCT (Sakura Finetek; 4583), frozen, and sectioned at 10 μm using a cryostat. Sections were fixed in 4% paraformaldehyde (PFA) for 8 min at RT followed by a 5 min wash in 1× PBS-T and blocking in "Block" or "NDS Block" for 15 min (see preceding paragraph). All antibodies were diluted in blocking solution and incubated at the conditions indicated (Table 2). Following primary antibody incubation, sections were rinsed 3 × 5 min in 1× PBS-T.

Tissue culture and mouse tissue; secondary antibody through mounting. All samples were incubated in secondary antibodies (Table 3) diluted in Block/NDS Block plus Hoechst (Invitrogen; H3570) for 15 min at RT. Samples were then washed 3 × 5 min in PBS-T. Coverslips were mounted with antifade solution (0.25% *p*-phenylenediamine, 10% 1× PBS, 90% glycerol, pH 9.0) and sealed with clear nail polish.

Spindle orientation analysis

For spindle orientation analysis of fixed cells, cells were plated on laminin-coated coverslips. Calcium (0.5 mM) was added 4 h before fixation to up-regulate cellular junctions and induce proliferation. FIJI (ImageJ) was used to process images. Spindle angles were measured using maximum-intensity projections of all z-slices that contained cortical spindle orientation machinery. Division angles were measured as the angle between spindle pole NuMA staining and the center of the cortical NuMA crescent. Only metaphase cells were used for analysis.

Antibody	Host	Supplier	Catalogue number	Fixative	Dilution	Incubation and notes
β-4 Integrin	Rat	BD Biosciences	553745	PFA	1:200	1 h, RT
α-Tubulin	Rat	Santa Cruz	sc-53029	MeOH/Glut	1:100	1 h, RT
Foxi3 (L-17)	Goat	Santa Cruz	sc-324865	PFA	1:100	1 h, RT
GFP	Chicken	Abcam	ab13970	MeOH/PFA	1:200	1 h or O/N, 4°C
KIF18B	Rabbit	Sigma	HPA024205	MeOH	1:100	O/N, 4°C. Preextract in 0.05% Triton-X for 30 s at 37°C
KIF18B	Gift	Medema Lab, Netherlands Cancer Institute	N/A	PFA	1:50	O/N, 4°C
LHX2 (C-20)	Goat	Santa Cruz,	sc-19344,	PFA	1:100	1 hr, RT
NuMA	Rabbit	Thermo Fisher	PA3-16829	MeOH	1:100	O/N, 4 °C
NuMA	Goat	Santa Cruz,	sc-51164	MeOH	1:100	O/N, 4 °C
$p150^{glued}$	Mouse	BD Biosciences,	610473	MeOH	1:100	O/N, 4 °C
Sox2	Rabbit	Abcam	ab92494	PFA	1:200	1 h, RT
Sox2	Rat	Invitrogen	14-9811-80	PFA	1:200	1 h, RT
Sox9	Rabbit	Millipore	Ab5535	PFA	1:1000	1 h, RT

TABLE 2: Primary antibody and immunofluorescence staining information.

For spindle orientation analysis of back skin tissue sections, division angles of basal cells were measured between NuMA-GFP puncta with respect to the basement membrane, marked by β-4 integrin. Placodes cells were identified by morphological characteristics and by Sox2 to mark the dermal condensate (Saxena *et al.*, 2019). Both metaphase and anaphase cells were used, as identified by their DNA condensation.

Time-lapse imaging

KIF18B;EB1-GFP control and KO primary keratinocytes were isolated from mouse back skin as described above and plated on 3.5 mm glass-bottomed tissue culture (TC) plates (MatTek Corporation; P35G-1.5-14-C) coated with laminin. Calcium (0.5 mM) was added 4 h ahead of imaging to up-regulate cellular junctions and induce proliferation. Cells were imaged on an Andor XD Revolution Spinning Disk Confocal with temperature control chamber (37°C) and CO_2 (5%) (Duke Light Microscopy Core Facility). Thirty-second movies (1 frame/second) were taken using a 60× Plan-Apo 1.2 NA water objective, Andor Ixon3 897 512 EMCCD camera, and MetaMorph Software. Postacquisition processing of movies was done with FIJI (ImageJ). EB1-GFP comets were tracked manually using the FIJI Manual Tracking Plugin. Ten EB1-GFP puncta were tracked per cell, five per spindle pole but across the entire astral region. The brightest puncta were selected for tracking.

Antibody	Catalogue number
Alexa Fluor 488 donkey anti-chicken	703-545-155
Alexa Fluor 488 donkey anti-goat	705-545-003
Alexa Fluor 488 Donkey anti-Rabbit	711-545-152
Alexa Fluor 488 donkey anti-rat	712-545-153
Alexa Fluor 647 donkey anti-rabbit	711-605-152
Alexa Fluor 647 donkey anti-rat	712-605-153
Rhodamine Red-X donkey anti-goat	705-295-147
Rhodamine Red-X donkey anti-mouse	715-295-151
Rhodamine Red-X donkey anti-rabbit	711-295-152
Rhodamine Red-X donkey antirRat	712-295-153

Jackson ImmunoResearch was the source for all. Also, the dilution for all was 1:200.

TABLE 3: Secondary antibody information.

Microscopy

All fluorescent images of fixed samples were taken using a Zeiss AxioImager Z1 microscope with an Apotome 2 attachment, PlanAPOCHROMAT 20× objective, 40×/1.3 oil objective, or Plan-NEOFLUAR 63×/1.4 oil objective and Axiocam 506 monocamera and Zeiss Zen Software. Images were processed using FIJI (ImageJ) and Adobe Photoshop.

Image quantification, graphing, and statistical analysis

Image quantifications were done using either the LI-COR Odyssey FC System (Western blot) or FIJI. All graphing and statistical analyses were done using Prism, except for spindle orientation analysis. Radial histograms for spindle orientation were done using MATLAB and analyzed for significance with a Kolmogorov–Smirnov test. All remaining data were statistically analyzed using a Student's unpaired *t* test.

ACKNOWLEDGMENTS

We thank Claire Walczak (Indiana University), René Medema (Netherlands Cancer Institute), and Purushothama Rao Tata (Duke University) for reagents. We thank Julie Underwood for care of the mice and the entire Lechler lab for their thoughtful comments throughout the course of this project and on the manuscript. This work was generously funded by a National Institutes of Health National Institute of Arthritis and Musculoskeletal and Skin Diseases NRSA F31 Predoctoral Fellowship (5F31AR074250) to R.S.M. and R01 (5R01AR067203) to T. L.

REFERENCES

Bendre S, Rondelet A, Hall C, Schmidt N, Lin YC, Brouhard GJ, Bird AW (2016). GTSE1 tunes microtubule stability for chromosome alignment and segregation by inhibiting the microtubule depolymerase MCAK. J Cell Biol 215, 631–647.

Box K, Joyce BW, Devenport D (2019). Epithelial geometry regulates spindle orientation and progenitor fate during formation of the mammalian epidermis. eLife 8, e47102.
Byrd KM, Lough KJ, Patel JH, Descovich CP, Curtis TA, Williams SE (2016). LGN plays distinct roles in oral epithelial stratification, filiform papilla morphogenesis and hair follicle development. Development 143, 2803–2817.
Clark JF, Dinsmore CJ, Soriano P (2020). A most formidable arsenal: genetic technologies for building a better mouse. Genes Dev 34, 1256–1286.
Compton DA, Luo C (1995). Mutation of the predicted p34cdc2 phosphorylation sites in NuMA impair the assembly of the mitotic spindle and block mitosis. J Cell Sci 108(Pt 2), 621–633.
Gupta ML Jr, Carvalho P, Roof DM, Pellman D (2006). Plus end-specific depolymerase activity of Kip3, a kinesin-8 protein, explains its role in positioning the yeast mitotic spindle. Nat Cell Biol 8, 913–923.
Kotak S, Busso C, Gonczy P (2012). Cortical dynein is critical for proper spindle positioning in human cells. J Cell Biol 199, 97–110.
Kulukian A, Fuchs E (2013). Spindle orientation and epidermal morphogenesis. Philos Trans R Soc Lond B Biol Sci 368, 20130016.
Lechler T, Fuchs E (2005). Asymmetric cell divisions promote stratification and differentiation of mammalian skin. Nature 437, 275–280.
Lee YM, Kim E, Park M, Moon E, Ahn SM, Kim W, Hwang KB, Kim YK, Choi W, Kim W (2010). Cell cycle-regulated expression and subcellular localization of a kinesin-8 member human KIF18B. Gene 466, 16–25.
Lu MS, Johnston CA (2013). Molecular pathways regulating mitotic spindle orientation in animal cells. Development 140, 1843–1856.
Matos I, Asare A, Levorse J, Ouspenskaia T, de la Cruz-Racelis J, Schuhmacher LN, Fuchs E (2020). Progenitors oppositely polarize WNT activators and inhibitors to orchestrate tissue development. eLife 9, e54304.
McHugh T, Gluszek AA, Welburn JPI (2018). Microtubule end tethering of a processive kinesin-8 motor Kif18b is required for spindle positioning. J Cell Biol 217, 2403–2416.
Meier ID, Bernreuther C, Tilling T, Neidhardt J, Wong YW, Schulze C, Streichert T, Schachner M (2010). Short DNA sequences inserted for gene targeting can accidentally interfere with off-target gene expression. FASEB J 24, 1714–1724.
Morita R, Sanzen N, Sasaki H, Hayashi T, Umeda M, Yoshimura M, Yamamoto T, Shibata T, Abe T, Kiyonari H, *et al.* (2021). Tracing the origin of hair follicle stem cells. Nature 594, 547–552.
Mou H, Vinarsky V, Tata PR, Brazauskas K, Choi SH, Crooke AK, Zhang B, Solomon GM, Turner B, Bihler H, *et al.* (2016). Dual SMAD signaling inhibition enables long-term expansion of diverse epithelial basal cells. Cell Stem Cell 19, 217–231.
Muroyama A, Seldin L, Lechler T (2016). Divergent regulation of functionally distinct gamma-tubulin complexes during differentiation. J Cell Biol 213, 679–692.
Nguyen-Ngoc T, Afshar K, Gönczy P (2007). Coupling of cortical dynein and G alpha proteins mediates spindle positioning in Caenorhabditis elegans. Nat Cell Biol 9, 1294–1302.
Niessen MT, Scott J, Zielinski JG, Vorhagen S, Sotiropoulou PA, Blanpain C, Leitges M, Niessen CM (2013). aPKClambda controls epidermal homeostasis and stem cell fate through regulation of division orientation. J Cell Biol 202, 887–900.
Nowak JA, Polak L, Pasolli HA, Fuchs E (2008). Hair follicle stem cells are specified and function in early skin morphogenesis. Cell Stem Cell 3, 33–43.
Okumura M, Natsume T, Kanemaki MT, Kiyomitsu T (2018). Dynein-dynactin-NuMA clusters generate cortical spindle-pulling forces as a multi-arm ensemble. eLife 7, e36559.
Ouspenskaia T, Matos I, Mertz AF, Fiore VF, Fuchs E (2016). WNT-SHH antagonism specifies and expands stem cells prior to niche formation. Cell 164, 156–169.
Poulson ND, Lechler T (2010). Robust control of mitotic spindle orientation in the developing epidermis. J Cell Biol 191, 915–922.
Poulson ND, Lechler T (2012). Asymmetric cell divisions in the epidermis. Int Rev Cell Mol Biol 295, 199–232.
Rezza A, Wang Z, Sennett R, Qiao W, Wang D, Heitman N, Mok KW, Clavel C, Yi R, Zandstra P, *et al.* (2016). Signaling networks among stem cell precursors, transit-amplifying progenitors, and their niche in developing hair follicles. Cell Rep 14, 3001–3018.
Rompolas P, Deschene ER, Zito G, Gonzalez DG, Saotome I, Haberman AM, Greco V (2012). Live imaging of stem cell and progeny behaviour in physiological hair-follicle regeneration. Nature 487, 496–499.
Saxena N, Mok KW, Rendl M (2019). An updated classification of hair follicle morphogenesis. Exp Dermatol 28, 332–344.
Seldin L, Muroyama A, Lechler T (2016). NuMA-microtubule interactions are critical for spindle orientation and the morphogenesis of diverse epidermal structures. eLife 5, e12504.
Seldin L, Poulson ND, Foote HP, Lechler T (2013). NuMA localization, stability, and function in spindle orientation involve 4.1 and Cdk1 interactions. Mol Biol Cell 24, 3651–3662.
Sennett R, Wang Z, Rezza A, Grisanti L, Roitershtein N, Sicchio C, Mok KW, Heitman NJ, Clavel C, Ma'ayan A, *et al.* (2015). An integrated transcriptome atlas of embryonic hair follicle progenitors, their niche, and the developing skin. Dev Cell 34, 577–591.
Silk AD, Holland AJ, Cleveland DW (2009). Requirements for NuMA in maintenance and establishment of mammalian spindle poles. J Cell Biol 184, 677–690.
Singh D, Schmidt N, Muller F, Bange T, Bird AW (2021). Destabilization of long astral microtubules via Cdk1-dependent removal of GTSE1 from their plus ends facilitates prometaphase spindleorientation. Curr Biol 31, 766–781.e768.
Smart IH (1970). Variation in the plane of cell cleavage during the process of stratification in the mouse epidermis. Br J Dermatol 82, 276–282.
Stout JR, Yount AL, Powers JA, Leblanc C, Ems-McClung SC, Walczak CE (2011). Kif18B interacts with EB1 and controls astral microtubule length during mitosis. Mol Biol Cell 22, 3070–3080.
Tanenbaum ME, Macurek L, van der Vaart B, Galli M, Akhmanova A, Medema RH (2011). A complex of Kif18b and MCAK promotes microtubule depolymerization and is negatively regulated by Aurora kinases. Curr Biol 21, 1356–1365.
van Heesbeen R, Raaijmakers JA, Tanenbaum ME, Halim VA, Lelieveld D, Lieftink C, Heck AJR, Egan DA, Medema RH (2017). Aurora A, MCAK, and Kif18b promote Eg5-independent spindle formation. Chromosoma 126, 473–486.
Vasioukhin V, Degenstein L, Wise B, Fuchs E (1999). The magical touch: genome targeting in epidermal stem cells induced by tamoxifen application to mouse skin. Proc Natl Acad Sci USA 96, 8551–8556.
Walczak CE, Zong H, Jain S, Stout JR (2016). Spatial regulation of astral microtubule dynamics by Kif18B in PtK cells. Mol Biol Cell 27, 3021–3030.
West DB, Engelhard EK, Adkisson M, Nava AJ, Kirov JV, Cipollone A, Willis B, Rapp J, de Jong PJ, Lloyd KC (2016). Transcriptome analysis of targeted mouse mutations reveals the topography of local changes in gene expression. PLoS Genet 12, e1005691.
Williams SE, Beronja S, Pasolli HA, Fuchs E (2011). Asymmetric cell divisions promote Notch-dependent epidermal differentiation. Nature 470, 353–358.
Williams SE, Ratliff LA, Postiglione MP, Knoblich JA, Fuchs E (2014). Par3-mInsc and Galphai3 cooperate to promote oriented epidermal cell divisions through LGN. Nat Cell Biol 16, 758–769.